Title

Stability of a Cylindrical Solute-Solvent Interface: Effect of Geometry, Electrostatics, and Hydrodynamics

Journal

SIAM Journal on Applied Mathematics, 75(3)

ISSN

0036-1399

Authors

Li, BO
Sun, Hui
Zhou, Shenggao

Publication Date

2015

DOI

10.1137/140972093

Peer reviewed

HHS Public Access

Author manuscript

SIAM J Appl Math. Author manuscript; available in PMC 2016 February 12.

Published in final edited form as:

SIAM J Appl Math. 2015 ; 75(3): 907–928. doi:10.1137/140972093.

STABILITY OF A CYLINDRICAL SOLUTE-SOLVENT INTERFACE: EFFECT OF GEOMETRY, ELECTROSTATICS, AND HYDRODYNAMICS*

BO LI[†], **HUI SUN**[‡], and **SHENGGAO ZHOU**[§]

BO LI: bli@math.ucsd.edu; HUI SUN: hus003@math.ucsd.edu; SHENGGAO ZHOU: s4zhou@math.ucsd.edu

[†]Department of Mathematics and NSF Center for Theoretical Biological Physics, University of California, San Diego, 9500 Gilman Drive, Mail code: 0112, La Jolla, CA 92093-0112, U.S.A

[‡]Department of Mathematics and NSF Center for Theoretical Biological Physics, University of California, San Diego, 9500 Gilman Drive, Mail code: 0112, La Jolla, CA 92093-0112, U.S.A

[§]Department of Mathematics and NSF Center for Theoretical Biological Physics, University of California, San Diego, 9500 Gilman Drive, Mail code: 0112, La Jolla, CA 92093-0112, U.S.A

Abstract

The solute-solvent interface that separates biological molecules from their surrounding aqueous solvent characterizes the conformation and dynamics of such molecules. In this work, we construct a solvent fluid dielectric boundary model for the solvation of charged molecules and apply it to study the stability of a model cylindrical solute-solvent interface. The motion of the solute-solvent interface is defined to be the same as that of solvent fluid at the interface. The solvent fluid is assumed to be incompressible and is described by the Stokes equation. The solute is modeled simply by the ideal-gas law. All the viscous force, hydrostatic pressure, solute-solvent van der Waals interaction, surface tension, and electrostatic force are balanced at the solute-solvent interface. We model the electrostatics by Poisson's equation in which the solute-solvent interface is treated as a dielectric boundary that separates the low-dielectric solute from the high-dielectric solvent. For a cylindrical geometry, we find multiple cylindrically shaped equilibrium interfaces that describe polymodal (e.g., dry and wet) states of hydration of an underlying molecular system. These steady-state solutions exhibit bifurcation behavior with respect to the charge density. For their linearized systems, we use the projection method to solve the fluid equation and find the dispersion relation. Our asymptotic analysis shows that, for large wavenumbers, the decay rate is proportional to wavenumber with the proportionality half of the ratio of surface tension to solvent viscosity, indicating that the solvent viscosity does affect the stability of a solute-solvent interface. Consequences of our analysis in the context of biomolecular interactions are discussed.

*This work was supported by the US National Science Foundation (NSF) through grant DMS-1319731, the Center for Theoretical Biological Physics through NSF grant PHY-0822283, and the National Institutes of Health through grant R01GM096188.

Keywords

Solute-solvent interfaces; surface energy; electrostatic interactions; dielectric boundary force; solvent hydrodynamics; linear stability; projection method

1. Introduction

The stability of a solute-solvent interface that separates biomolecules from its surrounding aqueous solvent is crucial to the conformation, dynamics, and function of an underlying biomolecular system. Such a solute-solvent interface is often treated as a dielectric boundary as the dielectric coefficient of a biomolecular region can be as low as 1 – 4 while that of water can be as high as 80 under normal conditions [25]. This boundary is the key quantity in a large class of implicit or continuum solvent models [17,21,22,31,40] that describe efficiently the effect of aqueous solvent to biomolecular processes, such as protein folding and molecular recognition [21, 27].

The geometry of a solute-solvent interface is set largely by the van der Waals (vdW) short-ranged repulsion between solute particles and solvent molecules, describing the effect of excluded volume of solute particles. But the interfacial surface energy, which measures the energetic cost of a solute breaking the surrounding network of water molecules, plays an important role in the hydrophobic interaction [5, 9, 30]. Due to the large jump of dielectric coefficient across the dielectric boundary, the electrostatic interaction between biomolecular charges, polarized solvent, and mobile ions generate a strong effective force on the dielectric boundary. It should be noted that electrostatic interactions in biomolecular systems can be efficiently modeled by Poisson's or the Poisson–Boltzmann equation [3, 6, 10, 18, 28, 35, 36]. Experimental and theoretical studies have also indicated that the solvent shear motion can induce protein conformational changes and the solvent viscosity can affect the kinetics of such changes [1, 24, 26, 32, 33, 37–39, 41].

In this work, we study how these vdW interactions, interfacial surface energy, electrostatics, and solvent fluid motion contribute to the stability of a model cylindrical solute-solvent interface, cf. Figure 1. Such an interface resembles that of a long α-helix, RNA, or DNA. Our model is adapted from that proposed in our previous work [43] (cf. also [44]), and consists of the following main elements:

1. The motion of the dielectric boundary $\Gamma(t)$ (t denotes time) is defined by

$$V_n = \mathbf{u} \cdot \mathbf{n}, \quad (1.1)$$

where V_n is the normal velocity, $\mathbf{u}$ is the velocity field of solvent fluid, and $\mathbf{n}$ is the unit normal at the boundary $\Gamma(t)$ pointing from the solute region Ω_m to the solvent region Ω_w.

2. The solvent fluid is assumed to be incompressible, and is described by the Stokes equation

$$\nabla \cdot \mathbf{u} = 0 \quad \text{and} \quad \mu_w \Delta \mathbf{u} - \nabla p_w = 0, \quad (1.2)$$

where μ_w and p_w are the dynamic viscosity and pressure of the solvent fluid. The pressure $p_m = p_m(t)$ of solute molecules is assumed to be spatially constant and described simply by the ideal-gas law:

$$p_m(t)\mathrm{Vol}(\Omega_m(t))=C_m, \quad (1.3)$$

where Vol $(\Omega_m(t))$ is the volume of solute region, and C_m is a constant independent of spatial and temporal variables but dependent on the temperature and amount of gas which are assumed to be constant.

3. The electrostatic potential φ solves a boundary-value problem of Poisson's equation

$$\nabla \cdot \varepsilon_\Gamma \nabla \phi = -\rho \quad (1.4)$$

defined in the entire region $\mathbb{R}^3$. Here, ρ is a given, fixed charge density, and ε_Γ is the dielectric coefficient defined by

$$\varepsilon_\Gamma = \begin{cases} \varepsilon_m = \varepsilon_m' \varepsilon_0 & \text{in } \Omega_m(t), \\ \varepsilon_w = \varepsilon_w' \varepsilon_0 & \text{in } \Omega_w(t), \end{cases} \quad (1.5)$$

where ε_0 is the vacuum permittivity, and ε_m' and ε_w' are the dielectric coefficients (i.e., relative permittivities) of the solute and solvent, respectively. These are positive constants and satisfy in general $\varepsilon_m' < \varepsilon_w'$. The electrostatic potential determines the normal component of effective dielectric boundary force [7, 8, 14, 29]

$$f_{ele} = \frac{1}{2}\left(\frac{1}{\varepsilon_w} - \frac{1}{\varepsilon_m}\right)|\varepsilon_\Gamma \nabla \phi \cdot \mathbf{n}|^2 + \frac{1}{2}(\varepsilon_m - \varepsilon_w)|(I - \mathbf{n} \otimes \mathbf{n})\nabla \phi|^2, \quad (1.6)$$

where I is the 3 × 3 identity matrix. Note that the electrostatic force always points in the direction from the high-dielectric solvent to low-dielectric solute.

4. At the solute-solvent interface $\Gamma(t)$, all the viscous force, hydrostatic pressure, surface tension, solute-solvent vdW interaction force, and electrostatic force are balanced:

$$2\mu_w D(\mathbf{u})\mathbf{n} + (p_m - p_w - 2\gamma_0 H + n_w U_{vdW} + f_{ele})\,\mathbf{n} = \mathbf{0}, \quad (1.7)$$

where $D(\mathbf{u}) = (\nabla \mathbf{u} + (\nabla \mathbf{u})^T)/2$ is the strain rate tensor, γ_0 is the constant surface tension, H is the mean curvature, n_w is the constant number density of solvent molecules, and U_{vdW} is a solute-solvent vdW interaction potential. Typical values of the parameters, such as μ_w, n_w, and γ_0, are given in Section 4. The magnitude of these forces (per unit area) can be of the order 0.1 ~ 10 $k_B T$/Å with k_B the Boltzmann constant and T absolute temperature.

We find multiple cylindrically shaped equilibrium interfaces that describe polymodal (e.g., dry and wet) states of hydration of an underlying molecular system [5, 9, 30]. For instance, a larger equilibrium cylinder is relatively drier as water molecules are excluded further away from the center line of the cylinder. These steady states exhibit bifurcation behavior with respect to the charge density. We linearize our system around such equilibrium interfaces, and solve the resulting linearized system by a fluid projection method together with special functions for the electrostatic potential. We seek the solutions to the linearized system in the form $A_k e^{\omega t+ikz}$, where for any given mode k, A_k is a constant, and a negative $\omega = \omega(k)$ implies the decay of the initial perturbation $A_k e^{ikz}$, indicating the linear stability. Let us denote by R_0 the radius of an underlying cylindrically shaped equilibrium interface. Our calculations lead to the dispersion relation

$$\begin{aligned}\omega(k) &= \frac{\omega_{\mathrm{air}}(k)+\omega_{\mathrm{surf}}(k)+\omega_{\mathrm{vdW}}(k)+\omega_{\mathrm{ele}}(k)}{\omega_{\mathrm{hyd}}} \\ &= -\frac{\gamma_0}{2\mu_{\mathrm{w}}}k+O(1) \quad \text{as } k \to \infty,\end{aligned} \tag{1.8}$$

where $\omega_{\mathrm{air}}(k)$, $\omega_{\mathrm{surf}}(k)$, $\omega_{\mathrm{vdW}}(k)$, $\omega_{\mathrm{ele}}(k)$, and ω_{hyd} are individual contributions from the solute air pressure (i.e., the term p_{m}), surface energy, vdW interaction, electrostatics, and hydrodynamics, respectively. They are given by

$$\begin{aligned}\omega_{\mathrm{air}}(k) &= -\frac{2C_m}{\pi L R_0^3}\chi_{\{k=0\}}(k), \\ \omega_{\mathrm{surf}}(k) &= \gamma_0 \left(\frac{1}{R_0^2}-k^2\right), \\ \omega_{\mathrm{vdW}}(k) &= n_{\mathrm{w}} U'_{\mathrm{vdW}}(R_0), \\ \omega_{\mathrm{ele}}(k) &= \frac{(\varepsilon_{\mathrm{w}}-\varepsilon_{\mathrm{m}})^2}{\varepsilon_{\mathrm{w}}\varepsilon_{\mathrm{m}}(\varepsilon_{\mathrm{w}}+\varepsilon_{\mathrm{m}})}\left[\fint_0^{R_0} s\rho(s)\mathrm{d}s\right]^2 k+O(1), \\ \omega_{\mathrm{hyd}}(k) &= 2\mu_{\mathrm{w}}k+O(1),\end{aligned}$$

as $k \to \infty$, where χ_A denotes the characteristic function of a set A and the symbol $\fint$ denotes an averaged integral (e.g., an integral over $[a, b]$ divided by $b - a$ in one-dimension).

Except the viscous force, all the static pressure, surface energy, vdW interaction, and electrostatics that are present in the force balance on the dielectric boundary (cf. (1.7)) are the main components in the recently developed variational implicit-solvent models (VISM) that have successfully predicted solvation free energies and different conformations of charged molecules. See [13, 15, 16, 19, 20, 23, 34, 42, 47, 48] and [4, 11, 12]. VISM centers around a solvation free-energy functional of all possible solute-solvent interfaces or dielectric boundaries Γ that separate the solvent region Ω_{w} from solute region Ω_{m}. A simple form of this functional is given by

$$G(\Gamma) = \Delta P\,\mathrm{Vol}\,(\Omega_{\mathrm{m}})+\gamma_0 \mathrm{Area}(\Gamma)+n_{\mathrm{w}}\int_{\Omega_{\mathrm{w}}} U_{\mathrm{vdW}}\, dV+G_{\mathrm{ele}}[\Gamma].$$

Here ΔP is the difference between solvent and solute pressures on the boundary Γ. The term $G_{\mathrm{ele}}[\Gamma]$ is the electrostatic free energy, defined to be the integral of $\rho\varphi/2$ over the entire system region with ρ being the charge density and φ the electrostatic potential that solves

Poisson's equation (1.4). The negative first variation $-\delta_\Gamma G[\Gamma]$ of the solvation free energy $G[\Gamma]$ with respect to the location change of boundary Γ defines the normal component of effective force on Γ:

$$F_n = -\delta_\Gamma G(\Gamma) = -\Delta P - 2\gamma_0 H + n_w U_{vdW} + f_{ele},$$

where $f_{ele} = -\delta_\Gamma G_{ele}[\Gamma]$ is given in (1.6). Therefore, the force balance (1.7) is exactly

$$2\mu_w D(\mathbf{u})\mathbf{n} + \delta_\Gamma G[\Gamma]\mathbf{n} = \mathbf{0}$$

on the interface with $\Delta P = p_w - p_m$. Note that we have implicitly assumed that the tangential components of the VISM force arising from the free energy $G[\Gamma]$ is negligible.

In our previous work [14], we studied the linear stability of a cylindrical dielectric boundary in the relaxation of surface energy and electrostatic energy. We found the dispersion relation $\omega(k) = -\gamma_0 k^2$ for $k \gg 1$. Our current work shows that the viscous effect of solvent fluid changes this dispersion relation to $\omega(k) = -\frac{\gamma_0}{2\mu_w} k$ for $k \gg 1$; cf. (1.8). This suggests that viscosity slows down the decay of interface perturbation for large modes k.

The rest of the paper is organized as follows: In Section 2, we describe in detail the governing equations of our solvent fluid dielectric boundary model. In Section 3, we obtain the steady-state solutions and their linearized equations for a cylindrical solute-solvent interface. Then we solve the linearized equations to obtain the dispersion relations. The details of derivation of the linearized system are presented in Appendix A. Some definitions and formulas for the modified Bessel functions are collected in Appendix B. In Section 4, we present numerical examples to show the contribution of each component to the stability. Finally, in Section 5, we draw our conclusions and discuss several possible directions of future work.

2. Governing Equations

We describe the cylindrical solute-solvent interface at time t by a smooth function $r = R(z, t)$ and assume it is L-periodic in z for some constant $L > 0$, where as usual $r = \sqrt{x^2 + y^2}$. With the cylindrical coordinates (r, θ, z), we define the solute-solvent interface $\Gamma(t)$, the solute region $\Omega_m(t)$, and the solvent region $\Omega_w(t)$ by

$$\begin{aligned}\Gamma(t) &= \{(r, \theta, z) \in \mathbb{R}^3 : r = R(z, t)\},\\ \Omega_m(t) &= \{(r, \theta, z) \in \mathbb{R}^3 : 0 \le r < R(z, t)\},\\ \Omega_w(t) &= \{(r, \theta, z) \in \mathbb{R}^3 : r > R(z, t)\},\end{aligned}$$

respectively, cf. Figure 1. Our governing equations are given by (1.1)–(1.4) and (1.7). We use the following boundary conditions ($\mathbf{x}$ denotes (x, y, z)): all $R(z, t)$, $\mathbf{u}(\mathbf{x}, t)$, $p_w(\mathbf{x}, t)$, and $\varphi(\mathbf{x}, t)$ are L-periodic in z; and $\mathbf{u} = \mathbf{0}$, $p_w = p_\infty$, and $\varphi = 0$ at $r = \infty$ and for all $z \in \mathbb{R}$.

The viscosity μ_w of solvent fluid, the number density of solvent molecules n_w, the pressure of solvent fluid $p_\infty > 0$ at infinity, and the surface tension $\gamma_0 > 0$ of the solute-solvent interface are all known constants. In the ideal-gas law, C_m is a positive constant independent of time t and spatial points. The dielectric coefficient ε_Γ is defined in (1.5), where the relative permittivities ε_m' for the solute and ε_w' for the solvent are known constants, satisfying $0<\varepsilon_m'<\varepsilon_w'$. We assume that the solute-solvent vdW interaction potential $U_{vdW} = U_{vdW}(r)$ is a given smooth function that depends only on r and that satisfies

$$U_{\mathrm{vdW}}(0)=\infty \quad \text{and} \quad U_{\mathrm{vdW}}(\infty)=0. \tag{2.1}$$

We also assume that the charge density $\rho = \rho(r) : \Omega \to \mathbb{R}$ in Poisson's equation is a known, continuous function that depends only on r. It is compactly supported: there exists $R_c > 0$ such that $\rho(r) = 0$ if $r > R_c$. Moreover, it satisfies the condition of charge neutrality:

$$\int_0^{R_c} r\rho(r)\,dr=0. \tag{2.2}$$

We now rewrite all the governing equations using the cylindrical coordinates. Let us first denote as usual by **i**, **j**, and **k** the cartesian coordinate vectors. For any point $\mathbf{x} = x\,\mathbf{i} + y\,\mathbf{j} + z\,\mathbf{k}$ with cylindrical coordinates (r, θ, z), where $r=\sqrt{x^2+y^2}$ and $\theta = \arctan y/x$, the local cylindrical basis (or coordinate) vectors are $\mathbf{e}_r = \cos\theta\,\mathbf{i}+\sin\theta\,\mathbf{j}$, $\mathbf{e}_\theta = -\sin\theta\,\mathbf{i} + \cos\theta\,\mathbf{j}$, and $\mathbf{e}_z = \mathbf{k}$. Note that $\mathbf{x} = r\mathbf{e}_r + z\mathbf{e}_z$. We assume that the velocity **u**, pressure p_w, and electrostatic potential φ at **x** are given by

$$\mathbf{u}(\mathbf{x},t)=u(r,z,t)\,\mathbf{e}_r+w(r,z,t)\,\mathbf{e}_z, \quad p_w=p_w(r,z,t), \quad \text{and} \quad \phi=\phi(r,z,t), \tag{2.3}$$

respectively. These, together with $r = R(z, t)$, are all the unknown functions in our equations. Note that the pressure $p_m(t)$ is eliminated as it can be readily expressed in terms of $R(z, t)$.

Our governing equations and boundary conditions for these unknown functions in the cylindrical coordinates are the following:

- Equations for interface motion:

$$\begin{cases} \partial_t R(z,t)=u(R(z,t),z,t)-w(R(z,t),z,t)\partial_z R(z,t) & \forall z\in\mathbb{R}, \\ R(z,t) \text{ is } L\text{- periodic in } z. \end{cases} \tag{2.4}$$

- Equations for solvent fluid:

$$\begin{cases} \mu_w\left(\partial_{rr}^2 u+\frac{1}{r}\partial_r u-\frac{1}{r^2}u+\partial_{zz}^2 u\right)-\partial_r p_w=0 & \text{if } r>R(z,t), \\ \mu_w\left(\partial_{rr}^2 w+\frac{1}{r}\partial_r w+\partial_{zz}^2 w\right)-\partial_z p_w=0 & \text{if } r>R(z,t), \\ \partial_r u+\frac{1}{r}u+\partial_z w=0 & \text{if } r>R(z,t), \\ u(r,z,t),\ w(r,z,t), \text{ and } p_w(r,z,t) \text{ are } L\text{- periodic in } z, \\ u(\infty,z,t)=w(\infty,z,t)=0 \text{ and } p_w(\infty,z,t)=p_\infty & \forall z\in\mathbb{R}. \end{cases} \tag{2.5}$$

- Poisson's equation for electrostatics:

$$\begin{cases} \varepsilon_{\mathrm{m}}\left(\partial_{rr}^2\phi+\frac{1}{r}\partial_r\phi+\partial_{zz}^2\phi\right)=-\rho \quad \text{in}\,\Omega_{\mathrm{m}}(t), \\ \varepsilon_{\mathrm{w}}\left(\partial_{rr}^2\phi+\frac{1}{r}\partial_r\phi+\partial_{zz}^2\phi\right)=-\rho \quad \text{in}\,\Omega_{\mathrm{w}}(t), \\ \phi(R(z,t)^-,z,t)=\phi(R(z,t)^+,z,t) \quad \forall z\in\mathbb{R}, \\ \varepsilon_{\mathrm{m}}\left[\partial_r\phi(R(z,t)^-,z,t)-\partial_z R(z,t)\partial_z\phi(R(z,t)^-,z,t)\right] \\ =\varepsilon_{\mathrm{w}}\left[\partial_r\phi(R(z,t)^+,z,t)-\partial_z R(z,t)\partial_z\phi(R(z,t)^+,z,t)\right] \quad \forall z\in\mathbb{R}, \\ \phi=\phi(r,z,t)\ \text{is}\ L\text{- periodic in}\ z, \\ \phi(\infty,z,t)=0 \quad \forall z\in\mathbb{R}, \end{cases} \tag{2.6}$$

where for a function $h = h(x)$, $h(x^-) = \lim_{y\to x-0} h(y)$ and $h(x^+) = \lim_{y\to x+0} h(y)$ are the left and right limits, respectively.

- Equations of force balance:

$$\begin{cases} \frac{2\mu_{\mathrm{w}}}{1+(\partial_z R)^2}\left[\partial_r u-\partial_z R(\partial_z u+\partial_r w)+(\partial_z R)^2\partial_z w\right]+\frac{C_{\mathrm{m}}}{\pi}\left[\int_0^L R(s,t)^2 ds\right]^{-1} \\ -p_{\mathrm{w}}-\gamma_0\left\{\frac{1}{R\left[1+(\partial_z R)^2\right]^{1/2}}-\frac{\partial_{zz}^2 R}{\left[1+(\partial_z R)^2\right]^{3/2}}\right\}+n_{\mathrm{w}}U_{\mathrm{vdW}}(R) \\ +\frac{1}{2}\left(\frac{1}{\varepsilon_{\mathrm{w}}}-\frac{1}{\varepsilon_{\mathrm{m}}}\right)\frac{\left[\varepsilon_{\Gamma(t)}\left(\partial_r\phi-\partial_z R\partial_z\phi\right)\right]^2}{1+(\partial_z R)^2} \\ +\frac{1}{2}(\varepsilon_{\mathrm{m}}-\varepsilon_{\mathrm{w}})\frac{(\partial_z R\partial_r\phi+\partial_z\phi)^2}{1+(\partial_r R)^2}=0 \quad \forall z\in\mathbb{R}, \\ \partial_z R\left(\partial_r u-\partial_z w\right)+\frac{1}{2}\left[1-(\partial_z R)^2\right](\partial_z u+\partial_r w)=0 \quad \forall z\in\mathbb{R}, \end{cases} \tag{2.7}$$

We now derive (2.4)–(2.7) from (1.1)–(1.7). If $\mathbf{x} = \mathbf{x}(t) \in \Gamma(t)$ has the cylindrical coordinates $(R(z, t), \theta, z)$, then

$$\mathbf{n}(\mathbf{x})=\frac{\mathbf{e}_r-\partial_z R\,\mathbf{e}_z}{\sqrt{1+(\partial_z R)^2}}, \quad \mathbf{n}^{\perp}=\frac{\partial_z R\,\mathbf{e}_r+\mathbf{e}_z}{\sqrt{1+(\partial_z R)^2}}, \quad \text{and} \quad \mathbf{e}_\theta \tag{2.8}$$

are orthonormal with $\mathbf{n}(\mathbf{x})$ the unit normal to $\Gamma(t)$. Since $\mathbf{x}(t) = R(z, t)\,\mathbf{e}_r + z\,\mathbf{e}_z$, the normal velocity at $\mathbf{x}$ is $V_n(\mathbf{x})=\dot{\mathbf{x}}\cdot\mathbf{n}(\mathbf{x})=\partial_t R/\sqrt{1+(\partial_z R)^2}$, where a dot denotes the time derivative. This, together with (1.1) and (2.3), leads to the first equation in (2.4).

By (2.3) and a series of calculations, we obtain for $\mathbf{x} \in \Omega_{\mathrm{w}}(t)$ the expression of $\Delta\mathbf{u}(\mathbf{x}, t)$ and $\nabla p_{\mathrm{w}}(\mathbf{x}, t)$ as linear combinations of $\mathbf{e}_r$ and $\mathbf{e}_z$. They lead to the Stokes equation, the first two equations, in (2.5). Similar calculations lead to the third equation in (2.5) for the incompressibility equation.

The gradient of $\varphi = \varphi(r, z, t)$ at $\mathbf{x} = r\mathbf{e}_r + z\mathbf{e}_z$ is $\nabla\varphi(\mathbf{x}, t) = \partial_r\varphi\,\mathbf{e}_r + \partial_z\varphi\,\mathbf{e}_z$. If $\mathbf{x} = \mathbf{x}(t) \in \Gamma(t)$ has the cylindrical coordinates $(R(z, t), \theta, z)$, then by (2.8) the normal derivatives of φ are given by

$$\partial_n\phi(\mathbf{x},t)=\nabla\phi(\mathbf{x},t)\cdot\mathbf{n}(\mathbf{x})=\frac{\partial_r\phi(R(z,t)^s,z,t)-\partial_z R(z,t)\partial_z\phi(R(z,t)^s,z,t)}{\sqrt{1+[\partial_z R(z,t)]^2}}, \tag{2.9}$$

where $s = -$ or $+$. Consequently, by these and the expression of Laplacian in cylindrical coordinates, we can rewrite the boundary-value problem of Poisson's equation (1.4) for the electrostatic potential $\varphi = \varphi(r, z, t)$ as the elliptic interface problem (2.6) [14, 28]. Note that the third and fourth equations in (2.6) are the continuities of the electrostatic potential φ and the normal component of electric displacement $-\varepsilon_{\Gamma(t)}\,\partial_n\varphi$, respectively, across the dielectric boundary $r = R(z, t)$.

To finally derive (2.7), we note that the volume $\mathrm{Vol}\,(\Omega_{\mathrm{m}}(t))$ of the cylindrical region $\Omega_{\mathrm{m}}(t)$ means that for one period $0 < z < L$. Since the cylindrical surface is represented by $r = R(z, t)$, the equation (1.3) for the ideal-gas law for the solute region is

$$p_{\mathrm{m}}(t)\int_0^L R(z,t)^2\,dz = \frac{C_{\mathrm{m}}}{\pi}. \quad (2.10)$$

If $\mathbf{x} = \mathbf{x}(t) \in \Gamma(t)$ has the cylindrical coordinates $(R(z, t), \theta, z)$, then direct calculations lead to

$$D(\mathbf{u}(\mathbf{x}))\mathbf{n}(\mathbf{x}) = \frac{1}{\sqrt{1+(\partial_z R)^2}}\left[\left(\partial_r u - \frac{1}{2}\partial_z R(\partial_z u + \partial_r w)\right)\mathbf{e}_r + \left(\frac{1}{2}(\partial_z u + \partial_r w) - \partial_z R\,\partial_z w\right)\mathbf{e}_z\right], \quad (2.11)$$

$$2H(\mathbf{x}) = -\frac{\partial_{zz}^2 R}{\left[1+(\partial_z R)^2\right]^{3/2}} + \frac{1}{R\left[1+(\partial_z R)^2\right]^{1/2}}. \quad (2.12)$$

By (2.8), (2.9), and (1.6), we have

$$f_{\mathrm{ele}}(\mathbf{x}) = \frac{1}{2}\left(\frac{1}{\varepsilon_{\mathrm{w}}} - \frac{1}{\varepsilon_{\mathrm{m}}}\right)\frac{\left[\varepsilon_{\Gamma(t)}(\partial_r\phi - \partial_z R\,\partial_z\phi)\right]^2}{1+(\partial_z R)^2} + \frac{1}{2}(\varepsilon_{\mathrm{m}} - \varepsilon_{\mathrm{w}})\frac{(\partial_z R\,\partial_r\phi + \partial_z\phi)^2}{1+(\partial_r R)^2}. \quad (2.13)$$

These, together with (2.11) and (2.10), allow us to rewrite the equation of force balance (1.7) on the boundary $\Gamma(t)$ into those in (2.7) by dotting (1.7) with $\mathbf{n}$ and $\mathbf{n}^{\perp}$, respectively. Note that each term in (2.7) is orthogonal to $\mathbf{e}_\theta$. The correspondence between terms in (1.7) and (2.7) is through the parameters μ_{w}, γ_0, n_{w}, etc.

3. Steady-State Solutions and Their Linear Stabilities

Steady-state solutions with cylindrical solute-solvent interfaces $r = R_0$ with constant radii $R_0 > 0$, together with their corresponding fluid velocity fields u_0, w_0, and pressures $p_{\mathrm{w}0}$, and the electrostatic potentials φ_0 are given by

$$
\begin{gathered}
r=R_0 \quad \forall z\in\mathbb{R},\\
u_0=w_0=0 \quad \text{for } r>R_0,\\
p_{\mathrm{w}0}=p_\infty \quad \text{for } r>R_0,\\
\phi_0(r)=\begin{cases} -\frac{1}{\varepsilon_{\mathrm{m}}}\int_0^r \frac{1}{s}\int_0^s \sigma\rho(\sigma)\,\mathrm{d}\sigma\mathrm{d}s+C_2 & \text{if } 0<r<R_0,\\ -\frac{1}{\varepsilon_{\mathrm{w}}}\int_{R_0}^r \frac{1}{s}\int_{R_0}^s \sigma\rho(\sigma)\,\mathrm{d}\sigma\mathrm{d}s+C_3\log r+C_4 & \text{if } r>R_0,\end{cases}\\
f(R_0):=\frac{C_{\mathrm{m}}}{\pi L R_0^2}-p_\infty-\frac{\gamma_0}{R_0}+n_{\mathrm{w}}U_{\mathrm{vdW}}(R_0)+\frac{1}{2}\left(\frac{1}{\varepsilon_{\mathrm{w}}}-\frac{1}{\varepsilon_{\mathrm{m}}}\right)\left[\hat{a}\acute{n}\dot{I}_0^{R_0} s\rho(s)\,ds\right]^2=0,
\end{gathered}
\tag{3.1}
$$

where

$$
\begin{cases}
C_2-C_3\log R_0-C_4=\frac{1}{\varepsilon_{\mathrm{m}}}\int_0^{R_0}\frac{1}{s}\int_0^s \sigma\rho(\sigma)\,\mathrm{d}\sigma\,\mathrm{d}s,\\
C_3=-\frac{1}{\varepsilon_{\mathrm{w}}}\int_0^{R_0} s\rho(s)\,\mathrm{d}s,\\
C_4=\lim_{r\to\infty}\left[\frac{1}{\varepsilon_{\mathrm{w}}}\int_{R_0}^r\frac{1}{s}\int_{R_0}^s \sigma\rho(\sigma)\,\mathrm{d}\sigma\,\mathrm{d}s-C_3\log r\right].
\end{cases}
$$

All R_0, u_0, w_0, $p_{\mathrm{w}0}$, and φ_0 satisfy the governing equations for the interface motion, fluid velocity and pressure, and electrostatics, and the corresponding boundary conditions. Eq. (3.1) is the force balance equation. The existence of $R_0 > 0$ such that $f(R_0) = 0$ follows from (2.1) together with the fact that $p_\infty > 0$ and $0 < \varepsilon_{\mathrm{m}} < \varepsilon_{\mathrm{w}}$. Note that if we consider the ordinary differential equation $\dot{R} = f(R)$ for $R = R(t)$, then the sign of $f'(R_0)$ determines the stability of R_0. The constants C_2, C_3, and C_4 are determined by the interface jump conditions and the boundary condition for the electrostatic potential φ_0 (cf. the third, fourth, and last equations in (2.6)). Note that the limit C_4 exists by the fact that the charge density $\rho = \rho(r)$ is compactly supported and by the charge neutrality (2.2).

We now linearize our system around a steady-state solution $r = R_0$, $u_0 = w_0 = 0$, $p_{\mathrm{w}0} = p_\infty$, and $\varphi_0 = \varphi_0(r)$ defined above. We assume

$$
\begin{cases}
R(z,t)=R_0+\delta R_1(z,t) & \text{for } z\in\mathbb{R},\\
u(r,z,t)=\delta u_1(r,z,t)+O(\delta^2) & \text{for } r>R(z,t),\\
w(r,z,t)=\delta w_1(r,z,t)+O(\delta^2) & \text{for } r>R(z,t),\\
p_{\mathrm{w}}(r,z,t)=p_\infty+\delta p_{\mathrm{w}1}(r,z,t)+O(\delta^2) & \text{for } r>R(z,t),\\
\phi(r,z,t)=\phi_0(r)+\delta\phi_1(r,z,t)+O(\delta^2) & \text{for } r\geq 0, z\in\mathbb{R},
\end{cases}
\tag{3.2}
$$

where $\delta\in\mathbb{R}$ is such that $|\delta| \ll 1$. All functions are L-periodic in z. Note that the expansion of velocity field is $\mathbf{u}(\mathbf{x}, t)+O(\delta^2) = \delta\mathbf{u}_1(\mathbf{x}, t)+O(\delta^2) = \delta[u_1(r, z, t)\,\mathbf{e}_r + w_1(r, z, t)\,\mathbf{e}_z]+ O(\delta^2)$, where $\mathbf{e}_r$, $\mathbf{e}_\theta$, and $\mathbf{e}_z$ are the local basis vectors at $\mathbf{x}$ that has cylindrical coordinates (r, θ, z).

The linearized equations and boundary conditions for R_1, u_1, w_1, $p_{\mathrm{w}1}$, and φ_1 are summarized below, and their derivations are detailed in Appendix A:

$$
\partial_t R_1(z,t)=u_1(R_0,z,t) \quad \forall z\in\mathbb{R}, \tag{3.3}
$$

$$\begin{cases} \mu_{\rm w}\left(\partial_{rr}^2 u_1+\frac{1}{r}\partial_r u_1-\frac{1}{r^2}u_1+\partial_{zz}^2 u_1\right)-\partial_r p_{w1}=0 \quad \text{for } r>R_0,\ z\in\mathbb{R}, \\ \mu_{\rm w}\left(\partial_{rr}^2 w_1+\frac{1}{r}\partial_r w_1+\partial_{zz}^2 w_1\right)-\partial_z p_{\rm w1}=0 \quad \text{for } r>R_0,\ z\in\mathbb{R}, \\ \partial_r u_1+\frac{1}{r}u_1+\partial_z w_1=0 \quad \text{for } r>R_0,\ z\in\mathbb{R}, \\ u_1(\infty,z,t)=w_1(\infty,z,t)=p_{\rm w1}(\infty,z,t)=0 \quad \forall z\in\mathbb{R}, \end{cases} \tag{3.4}$$

$$\begin{cases} \partial_{rr}^2\phi_1+\frac{1}{r}\partial_r\phi_1+\partial_{zz}\phi_1=0 \quad \text{if } r<R_0, \\ \partial_{rr}^2\phi_1+\frac{1}{r}\partial_r\phi_1+\partial_{zz}\phi_1=0 \quad \text{if } r>R_0, \\ \phi_1(R_0^+,z,t)-\phi_1(R_0^-,z,t)=-R_1(z,t)[\phi_0'(R_0^+)-\phi_0'(R_0^-)] \quad \forall z\in\mathbb{R}, \\ \varepsilon_{\rm m}\partial_r\phi_1(R_0^-,z,t)=\varepsilon_{\rm w}\partial_r\phi_1(R_0^+,z,t) \quad \forall z\in\mathbb{R}, \\ \phi_1(\infty,z,t)=0 \quad \forall z\in\mathbb{R}, \end{cases} \tag{3.5}$$

$$\begin{cases} 2\mu_{\rm w}\partial_r u_1(R_0,z,t)-\frac{2C_{\rm m}}{\pi LR_0^3}\int_0^L R_1(s,t)\,ds-p_{\rm w1}(R_0,z,t) \\ +\left(\frac{1}{\varepsilon_{\rm w}}-\frac{1}{\varepsilon_{\rm m}}\right)\varepsilon_{\rm w}^2\phi_0'(R_0^+)\left[R_1(z,t)\phi_0''(R_0^+)+\partial_r\phi_1(R_0^+,z,t)\right] \\ +\gamma_0\left(\partial_{zz}^2 R_1+\frac{R_1}{R_0^2}\right)+n_{\rm w}U'_{\rm vdW}(R_0)R_1=0 \quad \forall z\in\mathbb{R}, \\ \partial_r w_1(R_0,z,t)+\partial_z u_1(R_0,z,t)=0 \quad \forall z\in\mathbb{R}. \end{cases} \tag{3.6}$$

We now seek solutions to the linearized system (3.3)–(3.6) of the form

$$R_1(z,t)=e^{\omega t}e^{ikz},$$
$$(u_1(r,z,t),w_1(r,z,t),p_{\rm w1}(r,z,t),\phi_1(r,z,t))=e^{\omega t}e^{ikz}(\hat{u}_1(r),\hat{w}_1(r),\hat{p}_{\rm w1}(r),\hat{\phi}_1(r)),$$

where $k = 2\pi k'/L$ and k' is a nonnegative integer and all the functions $\hat{u}_1 = \hat{u}_1(r)$, $\hat{w}_1 = \hat{w}_1(r)$, $\hat{p_{\rm w1}} = \hat{p_{\rm w1}}(r)$, and $\hat{\varphi_1} = \hat{\varphi_1}(r)$ are to be determined. The sign of the growth rate $\omega = \omega(k)$ determines the linear stability of an underlying steady state. The system (3.3)–(3.6) reduces to

$$\omega=\hat{u}_1(R_0), \tag{3.7}$$

$$\begin{cases} \mu_{\rm w}\left[\hat{u}_1''+\frac{1}{r}\hat{u}_1'-\left(\frac{1}{r^2}+k^2\right)\hat{u}_1\right]-\hat{p}_{\rm w1}'=0 \quad \text{for } r>R_0, \\ \mu_{\rm w}\left(\hat{w}_1''+\frac{1}{r}\hat{w}_1'-k^2\hat{w}_1\right)-ik\hat{p}_{\rm w1}=0 \quad \text{for } r>R_0, \\ \hat{u}_1'+\frac{1}{r}\hat{u}_1+ik\hat{w}_1=0 \quad \text{for } r>R_0, \\ \hat{u}_1(\infty)=\hat{w}_1(\infty)=\hat{p}_{\rm w1}(\infty)=0, \end{cases} \tag{3.8}$$

$$\begin{cases} \hat{\phi}_1''+\frac{1}{r}\hat{\phi}_1'-k^2\hat{\phi}_1=0 \quad \text{for } r<R_0, \\ \hat{\phi}_1''+\frac{1}{r}\hat{\phi}_1'-k^2\hat{\phi}_1=0 \quad \text{for } r>R_0, \\ \hat{\phi}_1(R_0^+)-\hat{\phi}_1(R_0^-)=-[\phi_0'(R_0^+)-\phi_0'(R_0^-)], \\ \varepsilon_m\hat{\phi}_1'(R_0^-)=\varepsilon_{\rm w}\hat{\phi}_1'(R_0^+), \\ \hat{\phi}_1(\infty)=0, \end{cases} \tag{3.9}$$

$$\begin{cases} 2\mu_{\mathrm{w}}\hat{u}_1'(R_0)-\frac{2C_{\mathrm{m}}}{\pi LR_0^3}\chi_{\{k=0\}}-\hat{p}_{\mathrm{w}1}(R_0)+\gamma_0\left(\frac{1}{R_0^2}-k^2\right)+n_{\mathrm{w}}U'_{\mathrm{vdW}}(R_0) \\ \quad+\left(\frac{1}{\varepsilon_{\mathrm{w}}}-\frac{1}{\varepsilon_{\mathrm{m}}}\right)\varepsilon_{\mathrm{w}}^2\phi_0'(R_0^s)\left[\phi_0''(R_0^s)+\hat{\phi}_1'(R_0^s)\right]=0, \quad s=-\text{ or }+, \\ \hat{w}_1'(R_0)+ik\hat{u}_1(R_0)=0. \end{cases} \tag{3.10}$$

We shall use the modified Bessel functions of order n of the first and second kind $I_n(x)$ and $K_n(x)$. The definition and basic properties of these functions are recalled in Appendix B.

Lemma 3.1

The first three equations in (3.8) *together with the boundary conditions* (3.7)*, the fourth equation in* (3.8)*, and the second equation in* (3.10) *have a unique solution* $\hat{u}_1 = \hat{u}_1(r)$, $\hat{w}_1 = \hat{w}_1(r)$, $p_{\hat{\mathrm{w}}1} = p_{\hat{\mathrm{w}}1}(r)$*, given by*

$$\begin{aligned} &\textit{For } k=0: \quad \hat{u}_1(r)=\tfrac{R_0\omega}{r}, \quad \hat{w}_1(r)=0, \quad \textit{and} \quad \hat{p}_{\mathrm{w}1}(r)=0, \\ &\textit{For } k>0: \quad \begin{cases} \hat{u}_1(r)=\frac{\omega krK_0(kr)}{K_1(kR_0)}+\left[1-\frac{kR_0K_0(kR_0)}{K_1(kR_0)}\right]\frac{\omega K_1(kr)}{K_1(kR_0)}, \\ \hat{w}_1(r)=\frac{i\omega K_0(kr)}{K_1(kR_0)}\left[1+\frac{kR_0K_0(kR_0)}{K_1(kR_0)}\right]-\frac{i\omega krK_1(kr)}{K_1(kR_0)}, \\ \hat{p}_{\mathrm{w}1}(r)=\frac{2\omega\mu_{\mathrm{w}}kK_0(kr)}{K_1(kR_0)}. \end{cases} \end{aligned}$$

Proof—The case $k = 0$ can be proved by direct verifications. For the case $k > 0$, we use a projection method to find the solution in three steps.

Step 1: Let $a, b \in \mathbb{R}$. Consider the equations for the velocity components $\tilde{u}_1 = \tilde{u}_1(r)$ and $w_1\tilde{} = w_1\tilde{}(r)$:

$$\begin{gathered} \tilde{u}_1''+\tfrac{1}{r}\tilde{u}_1'-\left(\tfrac{1}{r^2}+k^2\right)\tilde{u}_1=0 \quad \text{for } r>R_0, \\ \tilde{w}_1''+\tfrac{1}{r}\tilde{w}_1'-k^2\tilde{w}_1=0 \quad \text{for } r>R_0, \\ \tilde{u}_1(R_0)=a, \quad \tilde{w}_1(R_0)=b, \quad \tilde{u}_1(\infty)=\tilde{w}_1(\infty)=0. \end{gathered}$$

By (B.5), the solution is given by

$$\tilde{u}_1(r)=a\frac{K_1(kr)}{K_1(kR_0)} \quad \text{and} \quad \tilde{w}_1(r)=b\frac{K_0(kr)}{K_0(kR_0)}. \tag{3.11}$$

Step 2: Find the general solution $p_1\tilde{} = p_1\tilde{}(r)$ to the equation

$$\tilde{p}_{\mathrm{w}1}''+\frac{1}{r}\tilde{p}_{\mathrm{w}1}'-k^2\tilde{p}_{\mathrm{w}1}=\tilde{u}_1'+\frac{1}{r}\tilde{u}_1+ik\tilde{w}_1 \tag{3.12}$$

and $p_{\tilde{\mathrm{w}}1}(\infty) = 0$. By (3.11) and (B.2), we can simplify the right-hand side of (3.12) as

$$\left[-\frac{ak}{K_1(kR_0)}+\frac{ikb}{K_0(kR_0)}\right] K_0(kr).$$

Since $K_0(kr)$ and $I_0(kr)$ are two linearly independent solutions to the homogeneous equation associated with (3.12) and their Wronskian is $1/r$ by (B.3) (the factor k does not appear), the general solution to (3.12) is then given by

$$\begin{aligned}\tilde{p}_{\mathrm{w}1}(r)=&\hat{C}_1\tfrac{K_0(kr)}{K_0(kR_0)}+\hat{C}_2\tfrac{I_0(kr)}{I_0(kR_0)}+\left[-\tfrac{ak}{K_1(kR_0)}+\tfrac{ikb}{K_0(kR_0)}\right]\\ &\cdot\left[-K_0(kr)\textstyle\int_{R_0}^{r} sI_0(ks)K_0(ks)\,\mathrm{d}s+I_0(kr)\int_{R_0}^{r} s(K_0(ks))^2\mathrm{d}s\right]\\ =&\hat{C}_1\tfrac{K_0(kr)}{K_0(kR_0)}+\hat{C}_2\tfrac{I_0(kr)}{I_0(kR_0)}+\left[-\tfrac{ak}{K_1(kR_0)}+\tfrac{ikb}{K_0(kR_0)}\right]\\ &\cdot\left\{-\tfrac{rK_1(kr)}{2k}+\tfrac{R_0^2}{2}[I_0(kR_0)K_0(kR_0)+I_1(kR_0)K_1(kR_0)]\,K_0(kr)\right.\\ &\left.-\tfrac{R_0^2}{2}[(K_0(kR_0))^2-(K_1(kR_0))^2]\,I_0(kr)\right\},\end{aligned}$$

where $\hat{C}_1$ and $\hat{C}_2$ are constants and where in the last step we used the formulas

$$\begin{aligned}\textstyle\int sI_0(s)K_0(s)\,\mathrm{d}s&=\tfrac{s^2}{2}[I_0(s)K_0(s)+I_1(s)K_1(s)],\\ \textstyle\int sK_0^2(s)\,\mathrm{d}s&=\tfrac{s^2}{2}[K_0^2(s)-K_1^2(s)],\end{aligned}$$

together with (B.2) and (B.3). These formulas can be directly verified by taking the derivatives of the right-hand sides and using (B.2) and (B.3).

It now follows from (B.5) and $\tilde{p_{\mathrm{w}1}}(\infty) = 0$ that

$$\hat{C}_2=\frac{R_0^2I_0(kR_0)}{2}\left[-\frac{ak}{K_1(kR_0)}+\frac{ikb}{K_0(kR_0)}\right][(K_0(kR_0))^2-(K_1(kR_0))^2].$$

Hence,

$$\tilde{p}_{\mathrm{w}1}(r)=\tilde{C}_1\frac{K_0(kr)}{K_0(kR_0)}-\left[-\frac{a}{2K_1(kR_0)}+\frac{ib}{2K_0(kR_0)}\right] rK_1(kr), \quad (3.13)$$

where

$$\tilde{C}_1=\hat{C}_1+\frac{R_0^2K_0(kR_0)}{2}\left[-\frac{ak}{K_1(kR_0)}+\frac{ikb}{K_0(kR_0)}\right]\cdot[I_0(kR_0)K_0(kR_0)+I_1(kR_0)K_1(kR_0)]$$

is a constant.

Step 3: Define

$$\begin{aligned}\hat{u}_1(r)&=\tilde{u}_1(r)-\tilde{p}'_{w1}(r),\\ \hat{w}_1(r)&=\tilde{w}_1(r)-ik\tilde{p}_{w1}(r),\\ \hat{p}_{w1}(r)&=-\mu_w\left[\tilde{p}''_{w1}(r)+\tfrac{1}{r}\tilde{p}'_{w1}(r)-k^2\tilde{p}_{w1}(r)\right].\end{aligned}$$

It is easy to verify that $\hat{u}_1$, $\hat{w}_1$, and $\hat{p_{w1}}$ satisfy the first three equations in (3.8). By (B.2) and (B.5), we can also verify that $\hat{u}_1(\infty)$, $\hat{w}_1(\infty)$, and $\hat{p_{w1}}(\infty)$ all equal 0. If we set $\tau_1 = -akK_0(kR_0)/K_1(kR_0) + ikb$ and $\tau_2 = b - ikC_1$, then we can verify by (3.11)–(3.13), together with (B.2), that

$$\begin{aligned}\hat{u}_1(r)&=-\tau_1\frac{2K_1(kr)+rkK_0(kr)}{2kK_0(kR_0)}+i\tau_2\frac{K_1(kr)}{K_0(kR_0)},\\ \hat{w}_1(r)&=\tau_1\frac{irK_1(kr)}{2K_0(kR_0)}+\tau_2\frac{K_0(kr)}{K_0(kR_0)},\\ \hat{p}_{w1}(r)&=-\mu_w\tau_1\frac{K_0(kr)}{K_0(kR_0)}.\end{aligned}$$

By (3.7) and the second equation in (3.10), we have

$$\begin{aligned}\left[\frac{K_1(kR_0)}{kK_0(kR_0)}+\frac{R_0}{2}\right]\tau_1-\tau_2\frac{iK_1(kR_0)}{K_0(kR_0)}&=-\omega,\\ \frac{iR_0}{2}\tau_1+\frac{K_1(kR_0)}{K_0(kR_0)}\tau_2&=i\omega.\end{aligned}$$

Solving these two equations, we get

$$\tau_1=-2k\omega\frac{K_0(kR_0)}{K_1(kR_0)}\quad\text{and}\quad\tau_2=\omega i\left[\frac{K_0(kR_0)}{K_1(kR_0)}+kR_0\frac{(K_0(kR_0))^2}{(K_1(kR_0))^2}\right].$$

Plugging τ_1 and τ_2 into $\hat{u}_1$, $\hat{w}_1$, and $\hat{p_{w1}}$ above, we obtain the desired solution expressions for the case $k > 0$.

Lemma 3.2

The solution $\hat{\varphi_1} = \hat{\varphi_1}(r)$ *to the system of equations and boundary conditions* (3.9) *for the electrostatic potential is given by*

$$\text{For } k=0:\quad \hat{\phi}_1(r)=\begin{cases}\phi_0'(R_0^+)-\phi_0'(R_0^-) & if\ 0<r<R_0,\\ 0 & if\ R_0<r<\infty.\end{cases}$$

$$\text{For } k>0:\quad \hat{\phi}_1(r)=\begin{cases}\frac{\varepsilon_w\,[\phi_0'(R_0^+)-\phi_0'(R_0^-)]\,K_1(kR_0)}{\varepsilon_m K_0(kR_0)I_1(kR_0)+\varepsilon_w I_0(kR_0)K_1(kR_0)}I_0(kr) & if\ 0<r<R_0,\\ -\frac{\varepsilon_m\,[\phi_0'(R_0^+)-\phi_0'(R_0^-)]\,I_1(kR_0)}{\varepsilon_m K_0(kR_0)I_1(kR_0)+\varepsilon_w I_0(kR_0)K_1(kR_0)}K_0(kr) & if\ R_0<r<\infty.\end{cases}$$

Proof—Direct verifications prove the result for the case $k = 0$. Fix $k > 0$. The solution $\hat{\varphi_1}(r)$ in each of the regions $r < R_0$ and $r > R_0$ is a linear combination of $I_0(kr)$ and $K_0(kr)$. By the last equation in (3.9) and by the asymptotic properties (B.4) and (B.5), we then have

$$\hat{\phi}_1(r)=\begin{cases} \overline{C}_1 I_0(kr) & \text{if } 0 \le r<R_0, \\ \overline{C}_2 K_0(kr) & \text{if } R_0<r<\infty, \end{cases}$$

where $\bar{C_1}$ and $\bar{C_2}$ are two constants. They are determined by the third and fourth equations in (3.9):

$$\begin{gathered} \overline{C}_2 K_0(kR_0)-\overline{C}_1 I_0(kR_0)=-[\phi_0'(R_0^+)-\phi_0'(R_0^-)], \\ \overline{C}_1 \varepsilon_{\mathrm{m}} I_1(kR_0)+\overline{C}_2 \varepsilon_{\mathrm{w}} K_1(kR_0)=0. \end{gathered}$$

where we used (B.2) in deriving the second equation. Solving for $\bar{C_1}$ and $\bar{C_2}$, we have the desired solution.

Proposition 3.3

The growth rate $\omega = \omega(k)$ is given by

$$\omega(k)=\frac{\omega_{\mathrm{air}}(k)+\omega_{\mathrm{surf}}(k)+\omega_{\mathrm{vdW}}(k)+\omega_{\mathrm{ele}}(k)}{\omega_{hyd}(k)}=-\frac{\gamma_0}{2\mu_{\mathrm{w}}}k+O(1), \quad (3.14)$$

where the asymptotics is with respect to $k \to \infty$ and

$$\begin{gathered} \omega_{\mathrm{air}}(k)=-\tfrac{2C_m}{\pi L R_0^3}\chi_{\{k=0\}}, \\ \omega_{\mathrm{surf}}(k)=\gamma_0\left(\tfrac{1}{R_0^2}-k^2\right), \\ \omega_{\mathrm{vdW}}(k)=n_{\mathrm{w}}U'_{\mathrm{vdW}}(R_0), \\ \omega_{\mathrm{ele}}(k)=\left(\tfrac{1}{\varepsilon_{\mathrm{w}}}-\tfrac{1}{\varepsilon_{\mathrm{m}}}\right)\left[\rho(R_0)\hat{a}\acute{n}\dot{I}_0^{R_0}s\rho(s)\,\mathrm{d}s-\tfrac{1}{R_0}\left(\hat{a}\acute{n}\dot{I}_0^{R_0}s\rho(s)\,\mathrm{d}s\right)^2\right] \\ +\tfrac{(\varepsilon_{\mathrm{w}}-\varepsilon_{\mathrm{m}})^2}{\varepsilon_{\mathrm{w}}\varepsilon_{\mathrm{m}}}\left[\hat{a}\acute{n}\dot{I}_0^{R_0}s\rho(s)\,\mathrm{d}s\right]^2\tfrac{kI_1(kR_0)K_1(kR_0)}{\varepsilon_{\mathrm{m}}K_0(kR_0)I_1(kR_0)+\varepsilon_{\mathrm{w}}I_0(kR_0)K_1(kR_0)} \\ =\tfrac{(\varepsilon_{\mathrm{w}}-\varepsilon_{\mathrm{m}})^2}{\varepsilon_{\mathrm{w}}\varepsilon_{\mathrm{m}}(\varepsilon_{\mathrm{w}}+\varepsilon_{\mathrm{m}})}\left[\hat{a}\acute{n}\dot{I}_0^{R_0}s\rho(s)\mathrm{d}s\right]^2k+O(1), \\ \omega_{\mathrm{hyd}}(k)=2\mu_{\mathrm{w}}\left[\tfrac{1}{R_0}+k^2R_0-\tfrac{k^2R_0(K_0(kR_0))^2}{(K_1(kR_0))^2}\right]=2\mu_{\mathrm{w}}k+O(1). \end{gathered}$$

We remark that the zeroth-mode mode perturbation ($k = 0$) is only in the r-direction. In this case, we have by taking the limit as $k \to 0$ and using (B.4) that

$$\begin{gathered} \omega_{\mathrm{ele}}(0)=\left(\tfrac{1}{\varepsilon_{\mathrm{w}}}-\tfrac{1}{\varepsilon_{\mathrm{m}}}\right)\left[\rho(R_0)\hat{a}\acute{n}\dot{I}_0^{R_0}s\rho(s)\,\mathrm{d}s-\tfrac{1}{R_0}\left(\hat{a}\acute{n}\dot{I}_0^{R_0}s\rho(s)\,\mathrm{d}s\right)^2\right], \\ \omega_{\mathrm{hyd}}(0)=\tfrac{2\mu_{\mathrm{w}}}{R_0}. \end{gathered}$$

The growth rate is then exactly

$$\omega(0)=\frac{R_0}{2\mu_{\mathrm{w}}}f'(R_0)$$
$$=\frac{R_0}{2\mu_{\mathrm{w}}}\left\{-\frac{2C_m}{\pi LR_0^3}1_{\{k=0\}}+\frac{\gamma_0}{R_0^2}+n_{\mathrm{w}}U'_{\mathrm{vdW}}(R_0)+\left(\frac{1}{\varepsilon_{\mathrm{w}}}-\frac{1}{\varepsilon_{\mathrm{m}}}\right)\left[\rho(R_0)\hat{a}\acute{n}\dot{I}_0^{R_0}s\rho(s)\,\mathrm{d}s-\frac{1}{R_0}\left(\hat{a}\acute{n}\dot{I}_0^{R_0}s\rho(s)\,\mathrm{d}s\right)^2\right]\right\},$$

where *f* is defined in (3.1).

Proof of Proposition 3.3—By Lemma 3.1,

$$2\mu_{\mathrm{w}}\hat{u}_1'(R_0)-\hat{p}_{\mathrm{w}1}(R_0)=-2\mu_{\mathrm{w}}\omega\left[\frac{1}{R_0}+k^2R_0-\frac{k^2R_0(K_0(kR_0))^2}{(K_1(kR_0))^2}\right].$$

For the steady-state electrostatic potential $\varphi_0 = \varphi_0(r)$, we have

$$\varepsilon_{\mathrm{w}}\phi_0'(R_0^+)=\varepsilon_{\mathrm{m}}\phi_0'(R_0^-)=-\hat{a}\acute{n}\dot{I}_0^{R_0}r\rho(r)\,dr.$$

By Lemma 3.2,

$$\hat{\phi}_1'(R_0^+)=\frac{\varepsilon_{\mathrm{m}}k\left[\phi_0'(R_0^+)-\phi_0'(R_0^-)\right]I_1(kR_0)K_1(kR_0)}{\varepsilon_{\mathrm{m}}K_0(kR_0)I_1(kR_0)+\varepsilon_{\mathrm{w}}I_0(kR_0)K_1(kR_0)}.$$

Plugging these and (A.2) into the first equation of (3.10) with *s* = +, we then obtain

$$\begin{aligned}&-2\mu_{\mathrm{w}}\omega\left[\frac{1}{R_0}+k^2R_0-\frac{k^2R_0(K_0(kR_0))^2}{(K_1(kR_0))^2}\right]-\frac{2C_m}{\pi LR_0^3}1_{\{k=0\}}\\&+\gamma_0\left(\frac{1}{R_0^2}-k^2\right)+n_{\mathrm{w}}U'_{\mathrm{vdW}}(R_0)\\&+\left(\frac{1}{\varepsilon_{\mathrm{w}}}-\frac{1}{\varepsilon_{\mathrm{m}}}\right)\left[\rho(R_0)\hat{a}\acute{n}\dot{I}_0^{R_0}s\rho(s)\,\mathrm{d}s-\frac{1}{R_0}\left(\hat{a}\acute{n}\dot{I}_0^{R_0}s\rho(s)\,\mathrm{d}s\right)^2\right]\\&+\frac{(\varepsilon_{\mathrm{w}}-\varepsilon_{\mathrm{m}})^2}{\varepsilon_{\mathrm{w}}\varepsilon_{\mathrm{m}}}\left[\hat{a}\acute{n}\dot{I}_0^{R_0}s\rho(s)\,\mathrm{d}s\right]^2\frac{kI_1(kR_0)K_1(kR_0)}{\varepsilon_{\mathrm{m}}K_0(kR_0)I_1(kR_0)+\varepsilon_{\mathrm{w}}I_0(kR_0)K_1(kR_0)}=0.\end{aligned}$$

This leads to the expression of growth rate $\omega = \omega(k)$ as desired.

Notice that $\omega_{\mathrm{hyd}}(k) > 0$ for all $k > 0$, since $0 < K_0(x) < K_1(x)$ for any $x > 0$ [2]. By (B.5),

$$\frac{K_0(kR_0)}{K_1(kR_0)}=1-\frac{1}{2kR_0}+O(k^{-2})\quad\text{and}\quad\frac{I_0(kR_0)}{I_1(kR_0)}=1+\frac{1}{2kR_0}+O(k^{-2})\quad\text{for } k\gg 1.$$

Thus,

$$\omega_{\mathrm{hyd}}(k)=2\mu_{\mathrm{w}}\left[\frac{1}{R_0}+k^2R_0-\frac{k^2R_0(K_0(kR_0))^2}{(K_1(kR_0))^2}\right]=2\mu_{\mathrm{w}}k+O(1).$$

Moreover,

$$\frac{kI_1(kR_0)K_1(kR_0)}{\varepsilon_{\mathrm{m}}K_0(kR_0)I_1(kR_0)+\varepsilon_{\mathrm{w}}I_0(kR_0)K_1(kR_0)}=\frac{k}{\varepsilon_{\mathrm{m}}+\varepsilon_{\mathrm{w}}}\left[1-\frac{\varepsilon_{\mathrm{w}}-\varepsilon_{\mathrm{m}}}{2kR_0(\varepsilon_{\mathrm{w}}+\varepsilon_{\mathrm{m}})}\right]+O(k^{-1}).$$

Therefore,

$$\omega_{\mathrm{ele}}(k)=\frac{(\varepsilon_{\mathrm{w}}-\varepsilon_{\mathrm{m}})^2}{\varepsilon_{\mathrm{w}}\varepsilon_{\mathrm{m}}(\varepsilon_{\mathrm{w}}+\varepsilon_{\mathrm{m}})}\left[\hat{a}\acute{n}\dot{I}_0^{R_0}s\rho(s)\mathrm{d}s\right]^2k+O(1)\quad \text{as } k\to\infty.$$

Combining all these, we obtain the desired asymptotics of $\omega(k)$.

4. Numerical Results

We use the following parameters that are typical values in molecular dynamics simulations:

$$T=298\,\mathrm{K},\quad \mu_{\mathrm{w}}=0.156\,\mathrm{k_B}T\cdot\mathrm{ps}/\text{Å}^3,\ n_{\mathrm{w}}=0.0331\ \text{Å}^{-3},\ p_\infty=2.46\times10^{-5}\mathrm{k_B}T/\text{Å}^3,$$
$$\gamma_0=0.175\,\mathrm{k_B}T/\text{Å}^2,\quad \varepsilon_0=1.4372\times10^{-4}\,\mathrm{e}^2/(\mathrm{k_B}T\cdot\text{Å}),\quad \varepsilon_{\mathrm{m}}=\varepsilon_0,\quad \varepsilon_{\mathrm{w}}=80\varepsilon_0,$$

where e is the elementary charge. We set the period L = 100 Å and the constant C_m = 0.65 $\mathrm{k_B}T$. We define

$$U_{\mathrm{vdW}}(r)=\kappa\left[\left(\frac{\sigma}{r}\right)^{11}-\left(\frac{\sigma}{r}\right)^{5}\right],$$

with κ = 5.0 $\mathrm{k_B}T$/Å^3 and σ = 10.0 Å. This potential is obtained by integrating a Lennard-Jones (LJ) 12-6 potential along the z-axis. We use an artificial charge density of the form (in the units e/Å^3)

$$\rho(r)=\rho_0\frac{R_c^4(2r-R_c)}{8r^4(r-R_c)^3}\exp\left(-\frac{R_c^4}{16r^2(r-R_c)^2}\right)\chi_{\{0\le r\le R_c\}}(r),$$

where ρ_0 (in the units e/Å) and R_c (in the units Å) are two positive numbers to be chosen later. One verifies that this charge density satisfies the charge neutrality condition (2.2), since

$$\int_0^r \rho(s) s \, \mathrm{d}s = \rho_0 \exp\left(-\frac{R_c^4}{16 r^2 (r - R_c)^2}\right) \chi_{\{r \le R_c\}}(r).$$

Note that the parameter ρ_0 sets the magnitude of the charge distribution and hence the electrostatic force. The parameter R_c determines the spatial range of electrostatic force. If we set R_c to be close to the LJ parameter σ, then a small variation of the value of R_c can result in a dramatical change of equilibrium radii.

We use Newton's method to solve (3.1) for R_0 (in the units Å), the radius of a cylindrically shaped equilibrium interface. For certain values of the parameter ρ_0, we find multiple values R_0 with different initial guesses in Newton's iteration. In Figure 2, we plot multiple branches of solutions R_0 vs. ρ_0 for (a) R_c = 10 Å and (b) R_c = 11.5 Å, respectively. Solid and dotted lines indicate stable and unstable branches of R_0, respectively, with respect to the zeroth-mode (k = 0) perturbation. For R_c = 10, there is a bifurcation at $\rho_0 = 5.04 \times 10^4$. For R_c = 11.5, there are two bifurcation points at $\rho_0 = 2.34 \times 10^4$ and $\rho_0 = 5.19 \times 10^4$, respectively. All these are saddle-node bifurcations.

We plot in Figure 3 the dispersion relation $\omega = \omega(k)$ given by (3.14) for R_c = 11.5. Figure 3 (a), (b), and (c) correspond to the data points on the bottom, middle, and top curves in Figure 2 (b), respectively. Let us first examine the stability and instability for the zeroth mode k = 0. From Figure 3 (a) and (c), we observe the zeroth-mode linear stability for all the parameter choices along the bottom or top curve in Figure 2 (b), and the instability for those along the middle curve in Figure 2 (b). Consider the increase of ρ_0 from the left bifurcation point from which the bottom and middle curves branch out in Figure 2 (b). We can see from Figure 3 (a) and (b) that the value of $\omega(0)$ along the bottom branch becomes more negative, indicating that the corresponding equilibrium shape is more stable. Along the middle branch, the value of $\omega(0)$ begins with 0 at the bifurcation point but rapidly increases to a large positive number and then gradually decreases to a small positive number near the right bifurcation point in Figure 2 (b). Consider now the decrease of ρ_0 from the right bifurcation point in Figure 2 (b) from which the top curve and middle curve branch out. We observe from Figure 3 (c) and (b) that the value of $\omega(0)$ becomes more negative along the top curve and more positive along the middle curve.

Let us now examine the general, nonzero mode k. Consider first the data points on the bottom curve in Figure 2 (b) from left to right as ρ_0 increases. Figure 3 (a) indicates that both the largest value of $\omega(k)$ and the range of the small-wavenumber instability increase. Consider now the data points on the middle branch in Figure 2 (b) from left to right as ρ_0 increases. We find from Figure 3 (b) the small-wavenumber instability and the large-wavenumber stability. As ρ_0 increases along the middle branch further to reach the right bifurcation point meeting with the top branch, the small-wavenumber instability diminishes and the interface switches its stability at the bifurcation. Finally, consider the top curve in Figure 2. We observe from Figure 2 (c) the linear stability for all wavenumbers k and for each data point on this curve. Moreover, for each k, $\omega(k)$ is more negative further away from the right bifurcation point. Note that the top branch terminates at the right bifurcation point

with $\rho_0 = 5.19 \times 10^4$ in Figure 2 (b). This indicates that for ρ_0 larger than this value, and $R_c = 11.5$, there is no equilibrium radius R_0 that is linearly stable for all wavenumbers.

Figure 4 displays the dispersion relations and contributions from different components of force corresponding to the three data points at $\rho_0 = 2.5\times10^4$ on the three branches, respectively, near but on the right of the left bifurcation point, in Figure 2 (b). Figure 4 (a) and (b) are for $0 \le k \le 3$ and $0 \le k \le 1500$, respectively. We observe for large k the linear decay of $\omega(k)$, the quadratic decay of $\omega_{\text{surf}}(k)$, and the linear growth of $\omega_{\text{hyd}}(k)$ and $\omega_{\text{ele}}(k)$, respectively, consistent with our asymptotic analysis summarized in Proposition 3.3. In the range of small wavenumbers k, the growth rate $\omega(k)$ increases with k for the top and bottom branches, but decreases with k for the middle branch. It is readily seen from Figure 4 (a) that, in the small k regime, the dispersion relation is dominated by $\omega_{\text{vdW}}(k)$ and $\omega_{\text{ele}}(k)$. The part $\omega_{\text{surf}}(k)$ is slightly positive for small k due to the cylindrical geometry but then drops quadratically. The part $\omega_{\text{ele}}(k)$ grows almost linearly with k except for $k \approx 0$ where there is some subtle nonlinearity. Hence $\omega_{\text{vdW}}(k)+\omega_{\text{ele}}(k)$ can be approximated as a linear function with a positive slope due to $\omega_{\text{ele}}(k)$. By diving $\omega_{\text{vdW}}(k) + \omega_{\text{ele}}(k)$ by $\omega_{\text{hyd}}(k)$, we find that the dispersion relation $\omega(k)$ can be approximately described by an inverse power law $\omega(k) \propto (c_1 + c_2/k)/\mu_{\text{w}}$, where c_1 and c_2 are constants depending on ρ_0 and R_c. This approximation is valid for k away from zero. For k close to zero, $\omega_{\text{hyd}} \approx 2\mu_{\text{w}}/R_0$. The effect of air pressure $\omega_{\text{air}}(k)$ is only reflected at $k = 0$, and it causes a negligibly small discontinuity at $k = 0$.

5. Conclusions

We have constructed a solvent fluid dielectric boundary model to describe the effect of solvent fluid to conformations of charged molecules in aqueous solution. In addition to the Stokes equation for the incompressible solvent fluid, we use the ideal-gas law to model solutes. Moreover, on the moving dielectric boundary, the viscous force balances the VISM forces that include hydrostatic pressures, surface tension, solute-solvent vdW interactions, and electrostatic force.

We have analyzed the linear stability of a steady-state cylindrical dielectric boundary. We find multiple such steady states that correspond to polymodal states (e.g., dry and wet) of hydration of charged molecules, as captured by our previous level-set variational implicit-solvent modeling [15,16,34,42,47,48]. Such nonuniqueness results from the competition between the surface tension, electrostatics, and solute-solvent vdW interactions. The multiple steady states bifurcate with respect to the charge distributions. Our stability analysis shows that the surface tension is the dominate effect in high-wavenumber stability. But the solvent viscosity weakens such stabilization as it changes the quadratic tail for large wavenumber to a linear one. The electrostatics always destablizes the system. The most important stability parameter we find is $\gamma_0/(2\mu_{\text{w}})$, half of the ratio of the surface tension γ_0 to the solvent fluid viscosity μ_{w}.

The instability of a solute-solvent interface is in fact a generic property of a real biomolecular system. For instance, the interface separating a protein from water molecules that are trapped inside the protein is metastable, as such water molecules lose their hydrogen bonding to the network of bulk water molecules [45, 46]. Our preliminary analysis only

indicates qualitatively the stabilizing factors, but does not characterize various scales at which the stability or instability occurs. It will be interesting to connect the small wavenumber instability analyzed here with the experiment and computer simulations on the metastable water molecules inside a protein.

The inclusion of solvent fluid flow is one step further to make an implicit-solvent approach more accurate in describing the important solvent effect. The development of numerical methods to solve our modeling system of equations is, however, nontrivial. One difficulty is to impose proper boundary conditions to allow solutes to change their volumes as occurring during the biomolecular conformational change. Usual boundary conditions, such as the periodic boundary condition imposed on the boundary of a computational region, will always keep the volume of solute region a constant because of the incompressibility of solvent fluid. A different issue is that the description of solutes by the ideal-gas law is over simplified. An improved approach is to include the solute molecular mechanical motion [16] and the coupling of such motion with the solvent fluid motion. Finally, our proposed solvent fluid model allows us to describe the solvent fluctuations through the Stokes equation with a stochastic stress tensor [43]. Such fluctuations are important in conformational changes of biomolecules. The mathematical description and numerical computation of such fluctuations will be challenging tasks.

Acknowledgments

We thank Dr. Michael White for many helpful discussions. We also thank Dr. Ray Luo for sending us the preprint [44].

References

1. Alexander-Katz A, Schneider MF, Schneider SW, Wixforth A, Netz RR. Shear-flow-induced unfolding of polymeric globules. Phys Rev Lett. 2006; 97:138101. [PubMed: 17026077]
2. Arfken, GB.; Weber, HJ.; Harris, FE. Mathematical Methods for Physicists: A Comprehensive Guide. 7. Elsevier; 2013.
3. Baker NA, Sept D, Joseph S, Holst MJ, McCammon JA. Electrostatics of nanosystems: Application to microtubules and the ribosome. Proc Natl Acad Sci USA. 2001; 98:10037–10041. [PubMed: 11517324]
4. Bates PW, Chen Z, Sun YH, Wei GW, Zhao S. Geometric and potential driving formation and evolution of biomolecular surfaces. J Math Biol. 2009; 59:193–231. [PubMed: 18941751]
5. Berne BJ, Weeks JD, Zhou R. Dewetting and hydrophobic interaction in physical and biological systems. Annu Rev Phys Chem. 2009; 60:85–103. [PubMed: 18928403]
6. Cai Q, Wang J, Hsieh MJ, Ye X, Luo R. Poisson–Boltzmann implicit solvation models. Annu Rep Comput Chem. 2012; 8:149–162.
7. Cai Q, Ye X, Luo R. Dielectric pressure in continuum electrostatic solvation of biomolecules. Phys Chem Chem Phys. 2012; 14:15917–15925. [PubMed: 23093365]
8. Cai Q, Ye X, Wang J, Luo R. Dielectric boundary forces in numerical Poisson–Boltzmann methods: Theory and numerical strategies. Chem Phys Lett. 2011; 514:368–373. [PubMed: 22125339]
9. Chandler D. Interfaces and the driving force of hydrophobic assembly. Nature. 2005; 437:640–647. [PubMed: 16193038]
10. Che J, Dzubiella J, Li B, McCammon JA. Electrostatic free energy and its variations in implicit solvent models. J Phys Chem B. 2008; 112:3058–3069. [PubMed: 18275182]
11. Chen Z, Baker NA, Wei GW. Differential geometry based solvation model I: Eulerian formulation. J Comput Phys. 2010; 229:8231–8258. [PubMed: 20938489]

12. Chen Z, Baker NA, Wei GW. Differential geometry based solvation model II: Lagrangian formulation. J Math Biol. 2011; 63:1139–1200. [PubMed: 21279359]
13. Cheng LT, Dzubiella J, McCammon JA, Li B. Application of the level-set method to the implicit solvation of nonpolar molecules. J Chem Phys. 2007; 127:084503. [PubMed: 17764265]
14. Cheng LT, Li B, White M, Zhou S. Motion of a cylindrical dielectric boundary. SIAM J Appl Math. 2013; 73:594–616. [PubMed: 23885130]
15. Cheng LT, Wang Z, Setny P, Dzubiella J, Li B, McCammon JA. Interfaces and hydrophobic interactions in receptor-ligand systems: A level-set variational implicit solvent approach. J Chem Phys. 2009; 131:144102. [PubMed: 19831428]
16. Cheng LT, Xie Y, Dzubiella J, McCammon JA, Che J, Li B. Coupling the level-set method with molecular mechanics for variational implicit solvation of nonpolar molecules. J Chem Theory Comput. 2009; 5:257–266. [PubMed: 20150952]
17. Cramer CJ, Truhlar DG. Implicit solvation models: Equilibria, structure, spectra, and dynamics. Chem Rev. 1999; 99:2161–2200. [PubMed: 11849023]
18. Davis ME, McCammon JA. Electrostatics in biomolecular structure and dynamics. Chem Rev. 1990; 90:509–521.
19. Dzubiella J, Swanson JMJ, McCammon JA. Coupling hydrophobicity, dispersion, and electrostatics in continuum solvent models. Phys Rev Lett. 2006; 96:087802. [PubMed: 16606226]
20. Dzubiella J, Swanson JMJ, McCammon JA. Coupling nonpolar and polar solvation free energies in implicit solvent models. J Chem Phys. 2006; 124:084905. [PubMed: 16512740]
21. Feig, M., editor. Modeling Solvent Environments: Applications to Simulations of Biomolecules. Wiley-VCH; 2010.
22. Feig M, Brooks CL III. Recent advances in the development and application of implicit solvent models in biomolecule simulations. Curr Opin Struct Biol. 2004; 14:217–224. [PubMed: 15093837]
23. Guo Z, Li B, Dzubiella J, Cheng LT, McCammon JA, Che J. Heterogeneous hydration of p53/MDM2 complex. J Chem Theory Comput. 2014; 10:1302–1313. [PubMed: 24803860]
24. Hagen SJ. Solvent viscosity and friction in protein folding dynamics. Curr Protein Pept Sci. 2010; 11:385–395. [PubMed: 20426733]
25. Hasted, JB. Aqueous Dielectrics. Chapman and Hall; London: 1973.
26. Klimov DK, Thirumalai D. Viscosity dependence of folding rates of protein. Phys Rev Lett. 1997; 79:317–320.
27. Levy Y, Onuchic J. Water mediation in protein folding and molecular recognition. Ann Rev Biophys Biomol Struct. 2006; 35:389–415. [PubMed: 16689642]
28. Li B. Minimization of electrostatic free energy and the Poisson–Boltzmann equation for molecular solvation with implicit solvent. SIAM J Math Anal. 2009; 40:2536–2566.
29. Li B, Cheng X-L, Zhang Z-F. Dielectric boundary force in molecular solvation with the Poisson–Boltzmann free energy: A shape derivative approach. SIAM J Applied Math. 2011; 71:2093–2111. [PubMed: 24058212]
30. Lum K, Chandler D, Weeks JD. Hydrophobicity at small and large length scales. J Phys Chem B. 1999; 103:4570–4577.
31. Roux B, Simonson T. Implicit solvent models. Biophys Chem. 1999; 78:1–20. [PubMed: 17030302]
32. Schneider SW, Nuschele S, Wixforth A, Gorzelanny C, Alexander-Katz A, Netz RR, Schneider MF. Shear-induced unfolding triggers adhesion of von Willebrand factor fibers. Proc Natl Acad Sci. 2007; 104:7899–7903. [PubMed: 17470810]
33. Sekhar A, Latham MP, Vallurupalli P, Kay LE. Viscosity-dependent kinetics of protein conformational exchange: Microviscosity effects and the need for a small viscogen. J Phys Chem B. 2014; 118:4546–4551. [PubMed: 24707961]
34. Setny P, Wang Z, Cheng LT, Li B, McCammon JA, Dzubliella J. Dewetting-controlled binding of ligands to hydrophobic pockets. Phys Rev Lett. 2009; 103:187801. [PubMed: 19905832]
35. Sharp KA, Honig B. Calculating total electrostatic energies with the nonlinear Poisson–Boltzmann equation. J Phys Chem. 1990; 94:7684–7692.

36. Sharp KA, Honig B. Electrostatic interactions in macromolecules: Theory and applications. Annu Rev Biophys Chem. 1990; 19:301–332.
37. Siedlecki CA, Lestini BJ, Kottke-Marchant KK, Eppell SJ, Wilson DL, Marchant RE. Shear-dependent changes in the three-dimensional structure of human von Willebrand factor. Blood. 1996; 88:2939–2950. [PubMed: 8874190]
38. Singh I, Themistou E, Porcar L, Neelamegham S. Fluid shear induces conformation change in human blood protein von Willebrand factor in solution. Biophys J. 2009; 96:2313–2320. [PubMed: 19289057]
39. Szymczak P, Cieplak M. Hydrodynamic effects in proteins. J Phys: Condens Matter. 2011; 23:033102. [PubMed: 21406855]
40. Tomasi J, Persico M. Molecular interactions in solution: An overview of methods based on continuous distributions of the solvent. Chem Rev. 1994; 94:2027–2094.
41. Vergauwe RMA, Uji-i H, De Ceunynck K, Vermant J, Vanhoorelbeke K, Hofkens J. Shear-stress-induced conformational changes of von Willebrand factor in water-glycerol mixture observed with single molecule microscopy. J Phys Chem B. 2014; 118:5660–5669. [PubMed: 24754487]
42. Wang Z, Che J, Cheng LT, Dzubiella J, Li B, McCammon JA. Level-set variational implicit solvation with the Coulomb-field approximation. J Chem Theory Comput. 2012; 8:386–397. [PubMed: 22346739]
43. White, MR.; Li, B. Solvent fluid motion with fluctuations and solute-solvent interface dynamics for charged molecules. 2014. (in preparation)
44. Xiao L, Cai Q, Li Z, Zhao H, Luo R. A multi-scale method for dynamics simulation in continuum solvent models. I: Finite-difference algorithm for Navier–Stokes equation. Chem Phys Lett. 2014; 616–617:67–74.
45. Yin H, Feng G, Clore GM, Hummer G, Rasaiah JC. Water in the polar and nonpolar cavities of the protein interleukin-1b. J Phys Chem B. 2010; 114:16290–7. [PubMed: 21047091]
46. Yin H, Hummer G, Rasaiah JC. Metastable water clusters in the nonpolar cavities of the thermostable protein tetrabrachion. Journal of the American Chemical Society. 2007; 129:7369–7377. [PubMed: 17508748]
47. Zhou S, Cheng L, Dzubiella J, Li B, McCammon JA. Variational implicit solvation with Poisson–Boltzmann theory. J Chem Theory Comput. 2014; 10:1454–1467. [PubMed: 24803864]
48. Zhou S, Rogers KE, de Oliveira CF, Baron R, Cheng LT, Dzubiella J, Li B, McCammon JA. Variational implicit-solvent modeling of host-guest binding: A case study on cucurbit[7]uril. J Chem Theory Comput. 2013; 9:4195–4204. [PubMed: 24039554]

Appendix A

In this appendix, we derive the linearized system (3.3)–(3.6). Equations (3.3) and (3.4) can be obtained simply by plugging the expansions (3.2) into (2.4) and (2.5), and matching the $O(\delta)$ terms. The first, second, and fifth equations in (3.5) can be obtained similarly using the corresponding equations in (2.6). At the interface $\Gamma(t)$ defined by $r = R(r, t)$ with $R(z, t)$ given in (3.2), we have

$$\begin{aligned}\phi(r,z,t)&=\phi\left(R_0+\delta R_1(z,t),z,t\right)\\&=\phi_0\left(R_0+\delta R_1(z,t)\right)+\delta\phi_1\left(R_0+\delta R_1(z,t),z,t\right)+O(\delta^2)\\&=\phi_0(R_0^s)+\delta\left[R_1(z,t)\phi_0'(R_0^s)+\phi_1(R_0^s,z,t)\right]+O(\delta^2)\quad \text{for } s=-\text{ or}+.\end{aligned}$$

Comparing $O(1)$-terms, we obtain the already known continuity $\phi_0(R_0^-)=\phi_0(R_0^+)$, cf. the third equation in (2.6) with φ_0 and R_0 replacing φ and $R(z, t)$, respectively. Comparing $O(\delta)$-terms, we obtain the third equation in (3.5), which is the first interface condition for φ_1 =

$\varphi_1(r, z, t)$. By (2.9), we have at either side $s = -$ or $+$ on the interface $r = R(z, t)$ defined in (3.2) that

$$\begin{aligned}\partial_n\phi(R(z,t)^s,z,t)&=\frac{\partial_r\phi(R(z,t)^s,z,t)-\partial_z R(z,t)\partial_z\phi(R(z,t)^s,z,t)}{\sqrt{1+[\partial_z R(z,t)]^2}}\\&=\phi_0'(R_0^s+\delta R_1(z,t))+\delta\partial_r\phi_1(R_0^s,z,t)+O(\delta^2)\\&=\phi_0'(R_0^s)+\delta\left[R_1(z,t)\phi_0''(R_0^s)+\partial_r\phi_1(R_0^s,z,t)\right]+O(\delta^2).\end{aligned}\tag{A.1}$$

Therefore, the $O(1)$-terms in the continuity of $\varepsilon_{\Gamma(t)}\partial_n\varphi$ at $r = R(z, t)$ (cf. the fourth equation in (2.6)) leads to the known continuity $\varepsilon_{\mathrm{m}}\phi_0'(R_0^-)=\varepsilon_{\mathrm{w}}\phi_0'(R_0^+)$. The $O(\delta)$-terms lead to

$$\varepsilon_{\mathrm{m}}\left[R_1(z,t)\phi_0''(R_0^-)+\partial_r\phi_1(R_0^-,z,t)\right]=\varepsilon_{\mathrm{w}}\left[R_1(z,t)\phi_0''(R_0^+)+\partial_r\phi_1(R_0^+,z,t)\right].$$

From the expression of the steady-state electrostatic potential φ_0, we have

$$\varepsilon_{\mathrm{m}}\phi_0''(R_0^-)=\varepsilon_{\mathrm{w}}\phi_0''(R_0^+)=\frac{1}{R_0}\hat{\mathrm{a}}\acute{\mathrm{n}}\mathrm{i}_0^{R_0}r\rho(r)\,dr-\rho(R_0).\tag{A.2}$$

These imply the fourth equation in (3.5) which is the second interface condition for φ_1.

To linearize the force balance equations (2.7), we first have by (3.2) and (2.10) that

$$p_{\mathrm{m}}(t)=\frac{C_{\mathrm{m}}}{\pi}\left[\int_0^L(R_0+\delta R_1(s,t))^2ds\right]^{-1}=\frac{C_{\mathrm{m}}}{\pi R_0^2L}-\delta\frac{2C_{\mathrm{m}}}{\pi LR_0^3}\hat{\mathrm{a}}\acute{\mathrm{n}}\mathrm{i}_0^L R_1(s,t)\,ds+O(\delta^2).$$

Now, at the interface $r = R(z, t)$, where a point has the cylindrical coordinates $(R(z, t), \theta, z)$, we have by (3.2) and (2.12), and routine calculations, that

$$\begin{gathered}\partial\alpha(R(z,t),z,t)=\delta\partial\alpha_1(R_0,z,t)+O(\delta^2),\quad \partial=\partial_r\text{ or }\partial_z\quad\text{and}\quad\alpha=u\text{ or }w,\\p_{\mathrm{w}}(R(z,t),z,t)=p_\infty+\delta p_{\mathrm{w}1}(R_0)+O(\delta^2),\\2H(R(z,t),\theta,z)=\tfrac{1}{R_0}-\delta\left(\partial_{zz}^2R_1+\tfrac{R_1}{R_0^2}\right)+O(\delta^2),\\n_{\mathrm{w}}U_{\mathrm{vdW}}(R(z,t))=n_{\mathrm{w}}U_{\mathrm{vdW}}(R_0)+\delta n_{\mathrm{w}}U_{\mathrm{vdW}}'(R_0)R_1(z,t)+O(\delta^2).\end{gathered}$$

Similarly, we have by (3.2) and (2.13) that

$$
\begin{aligned}
&f_{\mathrm{ele}}(R(z,t),z)\\
&+\tfrac{1}{2}\left(\tfrac{1}{\varepsilon_{\mathrm{w}}}-\tfrac{1}{\varepsilon_{\mathrm{m}}}\right)\tfrac{[\varepsilon_{\Gamma(t)}(\partial_r\phi-\partial_z R\partial_z\phi)]^2}{1+(\partial_z R)^2}+\tfrac{1}{2}(\varepsilon_{\mathrm{m}}-\varepsilon_{\mathrm{w}})\tfrac{(\partial_z R\partial_r\phi+\partial_z\phi)^2}{1+(\partial_r R)^2}\\
&=\tfrac{1}{2}\left(\tfrac{1}{\varepsilon_{\mathrm{w}}}-\tfrac{1}{\varepsilon_{\mathrm{m}}}\right)[\varepsilon_{\Gamma(t)}\partial_r\phi(R(z,t),z,t)]^2+O(\delta^2)\\
&=\tfrac{1}{2}\left(\tfrac{1}{\varepsilon_{\mathrm{w}}}-\tfrac{1}{\varepsilon_{\mathrm{m}}}\right)\varepsilon_{\mathrm{w}}^2[\phi_0'(R(z,t)^+)+\delta\partial_r\phi_1(R(z,t)^+,z,t)]^2+O(\delta^2)\\
&=\tfrac{1}{2}\left(\tfrac{1}{\varepsilon_{\mathrm{w}}}-\tfrac{1}{\varepsilon_{\mathrm{m}}}\right)\varepsilon_{\mathrm{w}}^2[\phi_0'(R_0^+)+\delta R_1(z,t)\phi_0''(R_0^+)+\delta\partial_r\phi_1(R_0^+,z,t)]^2+O(\delta^2)\\
&=\tfrac{1}{2}\left(\tfrac{1}{\varepsilon_{\mathrm{w}}}-\tfrac{1}{\varepsilon_{\mathrm{m}}}\right)[\varepsilon_{\mathrm{w}}\phi_0'(R_0^+)]^2\\
&+\delta\left(\tfrac{1}{\varepsilon_{\mathrm{w}}}-\tfrac{1}{\varepsilon_{\mathrm{m}}}\right)\varepsilon_{\mathrm{w}}^2\phi_0'(R_0^+)[R_1(z,t)\phi_0''(R_0^+)+\partial_r\phi_1(R_0^+,z,t)]+O(\delta^2).
\end{aligned}
$$

By the continuity of φ_0 at $r = R_0$, we can change ε_{w} and the sign + to ε_{m} and the sign −, respectively. All these, together with (2.7), imply the first equation in (3.6). The second equation in (3.6) can be obtained by straight forward calculations using (3.2).

Appendix B

We recall that the modified Bessel functions of order n of first and second kind, $I_n(x)$ and $K_n(x)$, are linearly independent solutions to the second-order equation [2]

$$y''+\frac{y'}{x}-\left(1+\frac{n^2}{x^2}\right)y=0. \quad \text{(B.1)}$$

Here we only consider nonnegative integers n. These functions satisfy the following properties [2]:

$$
\begin{aligned}
I_0'(x)&=I_1(x), \quad & I_1'(x)&=I_0(x)-\tfrac{I_1(x)}{x},\\
K_0'(x)&=-K_1(x), \quad & K_1'(x)&=-K_0(x)-\tfrac{K_1(x)}{x},
\end{aligned} \quad \text{(B.2)}
$$

$$W[I_0(x),K_0(x)]=I_0(x)K_0'(x)-I_0'(x)K_0(x)=\frac{1}{x}, \quad \text{(B.3)}$$

$$
\begin{aligned}
&I_n(s)\sim\tfrac{s^n}{2^n n!}, \quad K_n(s)=\tfrac{2^{n-1}(n-1)!}{s^n}(n\geq 1),\\
&K_0(s)\sim-\ln s, \quad \text{as } s\to 0^+,
\end{aligned} \quad \text{(B.4)}
$$

$$
\begin{aligned}
&I_n(s)\sim\tfrac{e^s}{\sqrt{2\pi s}}\left[1-\tfrac{4n^2-1}{8s}+O\left(\tfrac{1}{s^2}\right)\right],\\
&K_n(s)=\sqrt{\tfrac{\pi}{2s}}e^{-s}\left[1+\tfrac{4n^2-1}{8s}+O\left(\tfrac{1}{s^2}\right)\right], \quad \text{as } s\to\infty.
\end{aligned} \quad \text{(B.5)}
$$

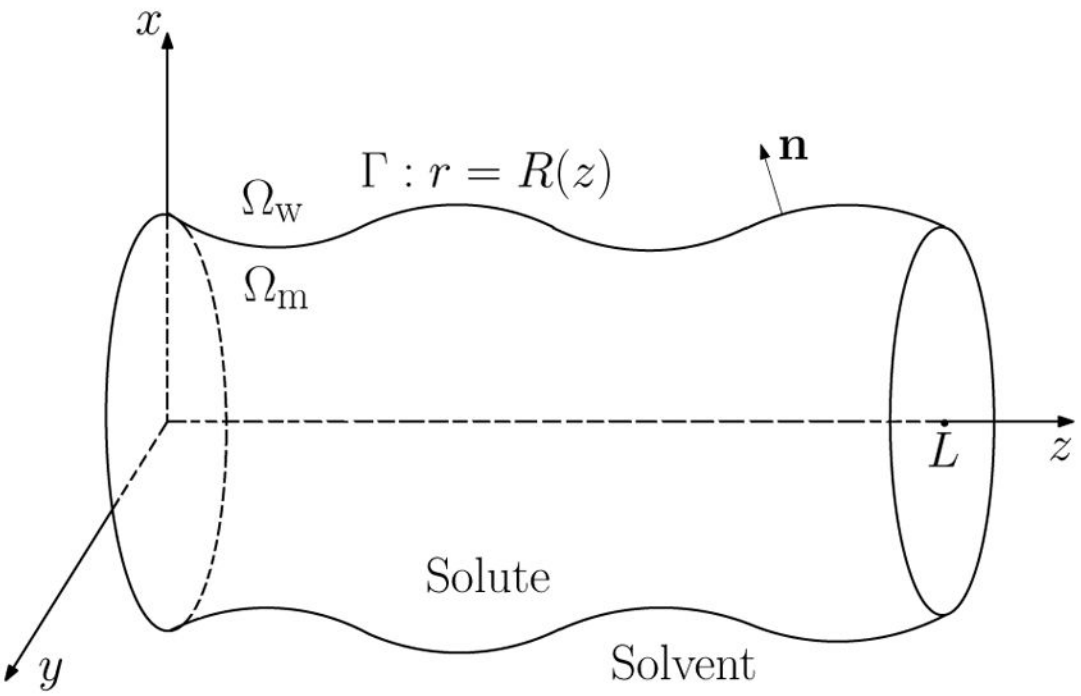

Fig. 1. A cylindrical solute-solvent interface

Γ *separates the interior solute region* Ω_m *(m stands for molecules) from the exterior solvent region* Ω_w *(w stands for water). The unit normal* **n** *at* Γ *points from* Ω_m *to* Ω_w. *The system is L-periodic in the z-axis, the axis of cylinder.*

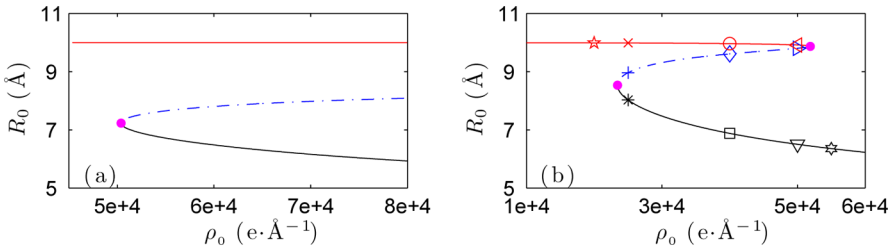

Fig. 2. Equilibrium radii R_0 vs. the parameter ρ_0 in the charge density ρ and their stabilities for the mode k

= 0 *with (a)* R_c = 10 *and (b)* R_c = 11.5. *Multiple values of* R_0 *are found for* ρ_0 *in certain ranges. Solid and dotted lines indicate the stable and unstable branches of* R_0, *respectively. The small magenta solid circles correspond to the saddle-node bifurcation points. In (b), the marker points in red, blue, and black from different branches correspond to the plots of dispersion relations in* Figures 3 and 4.

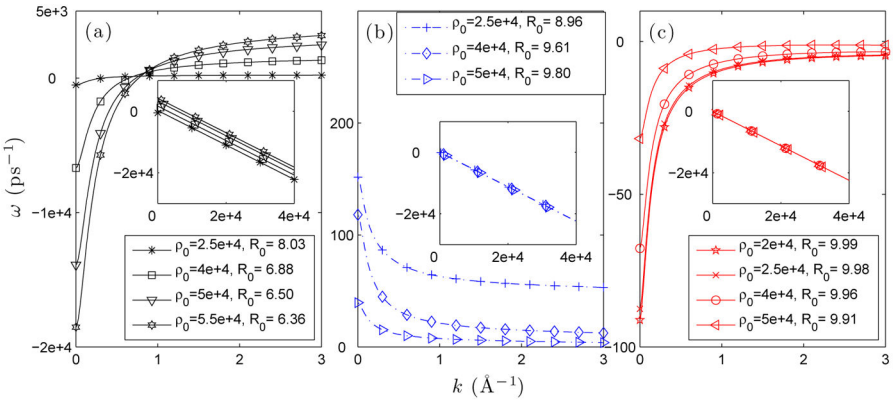

Fig. 3. Plots of the dispersion relations for multiple solutions R_0 with R_c = 11.5. *The four curves in (a) correspond to the four data points on the bottom curve in* Figure 2 (b). The three curves in (b) correspond to the three data points on the middle curve in Figure 2 (b). The four curves in (c) correspond to the four data points on the top curve in Figure 2 (b). Plots in each inset are for a large range of k.

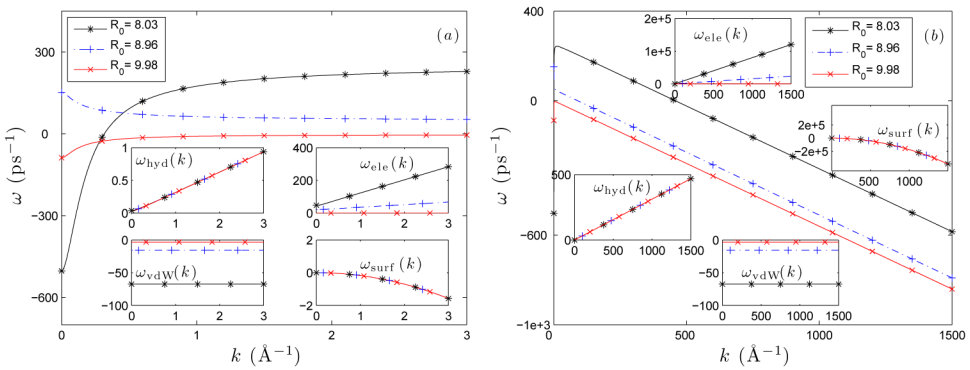

Fig. 4. The dispersion relations for multiple solutions of R_0 at ρ

$_0 = 2.5 \times 10^4$ *and* $R_c = 11.5$ *that correspond to the same marker points in* Figure 2 (b). The insets indicate different contributions to the growth rate ω(*k*) : *(a) Small range of k; (b) Large range of k.*